Crystal structures of human cardiac β-myosin II S2-Δ provide insight into the functional role of the S2 subfragment

Wulf Blankenfeldt*†‡, Nicolas H. Thomä*§, John S. Wray†, Mathias Gautel*¶, and Ilme Schlichting*†‡

*Max Planck Institute of Molecular Physiology, Department of Physical Biochemistry, 44227 Dortmund, Germany; †Max Planck Institute for Medical Research, Department of Biomolecular Mechanisms, 69120 Heidelberg, Germany; and ¶King's College London, Department of Muscle Cell Biology, The Randall Centre, New Hunt's House, SE 1 UL London, United Kingdom

Edited by James A. Spudich, Stanford University School of Medicine, Stanford, CA, and approved September 19, 2006 (received for review August 4, 2006)

Myosin II is the major component of the muscle thick filament. It consists of two N-terminal S1 subfragments ("heads") connected to a long dimeric coiled-coil rod. The rod is in itself twofold symmetric, but in the filament, the two heads point away from the filament surface and are therefore not equivalent. This breaking of symmetry requires the initial section of the rod, subfragment 2 (S2), to be relatively flexible. S2 is an important functional element, involved in various mechanisms by which the activity of smooth and striated muscle is regulated. We have determined crystal structures of the 126 N-terminal residues of S2 from human cardiac β-myosin II (S2-Δ), of both WT and the disease-associated E924K mutant. S2-Δ is a straight parallel dimeric coiled coil, but the N terminus of one chain is disordered in WT-S2-Δ due to crystal contacts, indicative of unstable local structure. Bulky noncanonical side chains pack into a/d positions of S2-Δ's N terminus, leading to defined local asymmetry and axial stagger, which could induce nonequivalence of the S1 subfragments. Additionally, S2 possesses a conserved charge distribution with three prominent rings of negative potential within S2-Δ, the first of which may provide a binding interface for the "blocked head" of smooth muscle myosin in the OFF state. The observation that many disease-associated mutations affect the second negatively charged ring further suggests that charge interactions play an important role in regulation of cardiac muscle activity through myosin-binding protein C.

coiled coil | muscle | crystallography | regulation | familial hypertrophic cardiomyopathy

Muscle contraction results from the ATP-dependent cyclic interaction of the proteins myosin II and actin, assembled in thick and thin filaments, respectively. Myosin II consists of two heavy chains, each of which binds one essential and one regulatory light chain (Fig. 1). The mechanical events underlying muscle contraction mainly involve the heavy chains: their N-terminal S1 subfragments or "crossbridges" act as ATP-driven motors whose conformation and actin affinity change depending on the status of their ATPase site (1). A 54-kDa coiled-coil region termed subfragment 2 (S2) connects the S1 "heads" to the thick filament backbone, in which the C-terminal coiled-coil light meromyosin (LMM) tails of individual myosin II molecules are packed side by side. Both heads point away from the thick filament surface and are therefore nonequivalent with respect to the LMM dimerization axis; they can take up highly regular arrangements, which in some muscles are involved in regulation (2). The S2 region is generally thought to be flexible to make nonequivalence possible and because the inner ends of the crossbridges would be far apart if both S1 heads attached without distortion to actin in the rigor state (but see ref. 3). S2, however, is more than just a flexible linker between S1 and LMM. In smooth muscle, S2's N-terminal 15 coiled-coil heptad repeats play a role in the regulation of activity (4). In addition, in striated muscle, S2 is a binding partner of myosin-binding protein C (MyBP-C; refs. 5 and 6), a modulator of sarcomere contractility (7). The physiological importance of S2 is further evidenced by point mutations leading to a heart disease known as familial hypertrophic cardiomyopathy (FHC or HCM; ref. 8).

Despite its importance, little is known about the structure of S2; the only crystal structure so far reported is that of a 51-residue fragment of scallop myosin (S2N51) fused to the leucine zipper of yeast transcription factor GCN4, which is a strong coiled-coil inducer (9). Because the presence of such an inducer can propagate coiled-coil formation over long distances (10), and because regulation in smooth-muscle myosin II requires the presence of at least 15 heptads (4), the chimeric S2N51 construct may not reveal important structural and functional features of S2. To gain further insight into the S2 region, and because of its clinical importance, we have determined crystal structures of the native N-terminal 126 residues of S2 from human cardiac β-myosin II (S2-Δ, P838–K963, covering ≈30% of the complete S2 subfragment) and its FHC-associated mutant E924K to 2.7- and 2.5-Å resolution, respectively. In addition to revealing mechanisms of asymmetry generation within S2-Δ, these two structures provide insight into the stabilization of the OFF state in smooth muscle myosin, even though cardiac and smooth muscle myosin are not regulated in the same way. Finally, a comparison of the structures of WT and E924K-S2-Δ together with an analysis of known FHC mutations (8) and the results of interactions studies (5) throws light on the regulatory function of MyBP-C in striated muscle.

Results and Discussion

Overall Structure. α-Helical coiled coils are versatile structural elements with prominent roles in many structural proteins, including those of muscle. They possess characteristic heptad sequence repeats in which the a and d positions are occupied by small hydrophobic residues, in dimeric coiled coils, typically valine at position a and leucine at position d (11). This generates a hydrophobic seam that holds the α-helices together with a and d positions interlocked in a symmetrical "knobs-into-holes" packing. At the same time, this interaction leads to a left-handed winding of individual chains around each other (12). Additional

Author contributions: W.B., N.H.T., M.G., and I.S. designed research; W.B., N.H.T., and I.S. performed research; W.B., N.H.T., and I.S. analyzed data; and W.B., J.S.W., M.G., and I.S. wrote the paper.

The authors declare no conflict of interest.

This article is a PNAS direct submission.

Abbreviations: S2-Δ, residues P838–K963 of the S2 subfragment of human cardiac β-myosin II; LMM, light meromyosin; FHC, familial hypertrophic cardiomyopathy.

Data deposition: The atomic coordinates and structure factor amplitudes have been deposited in the Protein Data Bank, www.pdb.org [PDB ID codes 2FXM (WT-S2-Δ) and 2FXO (E924K-S2-Δ)].

‡To whom correspondence may be addressed. E-mail: wulf.blankenfeldt@mpi-dortmund.mpg.de or ilme.schlichting@mpimf-heidelberg.mpg.de.

§Present address: Friedrich Miescher Institute, 4058 Basel, Switzerland.

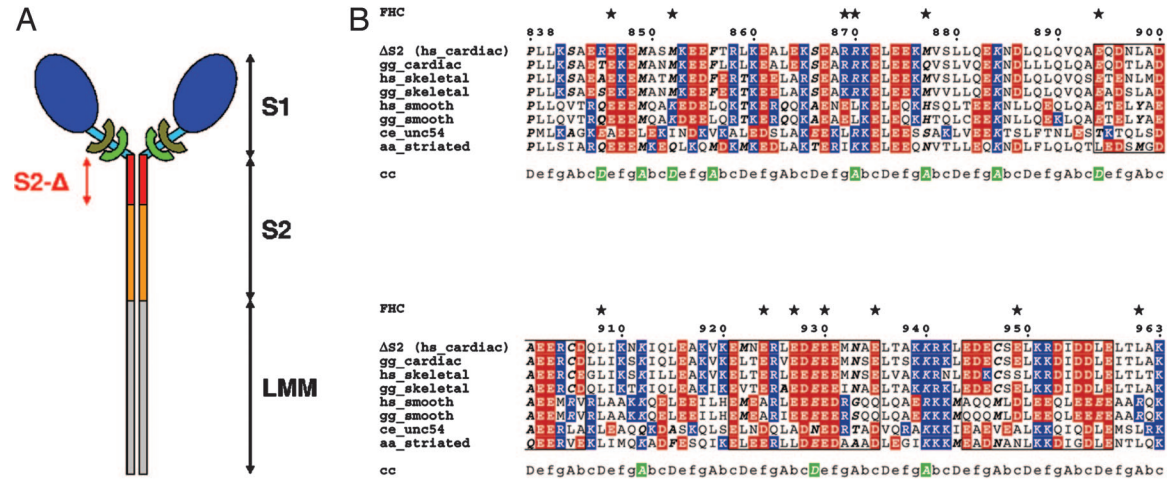

Fig. 1. Localization of S2-Δ in myosin II and comparison of various S2-Δ sequences. (*A*) Organization of the myosin II molecule. S1, subfragment 1 containing the ATPase domain (dark blue) and the regulatory domain consisting of lever arm (light blue) and essential (ELC) and regulatory light chain (RLC, shown in dark and light green, respectively); S2, subfragment 2 with S2-Δ highlighted in red; LMM in gray. The sketch is to approximate scale only. (*B*) Alignment of the N termini of several representative S2 sequences. The sequence numbering refers to S2-Δ. Acidic and basic residues are shaded in red and blue, respectively. Noncanonical residues in a/d positions of the coiled coil are shown in italicized bold characters. a/d positions occupied by large noncanonical residues in the majority of sequences shown are indicated by green shades of the coiled-coil ruler (cc). Black boxes show the three negative charge rings of S2-Δ (E894–D906, E921–E935, and E944–E958). Positions of previously identified FHC amino acid substitutions (FHC) are indicated by a star (*). The sequences represent myosin heavy chains from vertebrates and invertebrates, different tissue and with different regulatory properties. S2-Δ, human cardiac β-myosin II (MYH7_HUMAN; UniProtKB accession no. P12883); gg_cardiac, chicken cardiac (MYSC_CHICK; P29616); hs_skeletal, human skeletal (MYH13_HUMAN, Q9UKX3); gg_skeletal, adult chicken skeletal (MYSS_CHICK, P13538); hs_smooth, human smooth muscle (MYH11_HUMAN, P35749); gg_smooth, chicken gizzard (MYH11_CHICK, P10587); ce_unc54, *Caenorhabditis elegans* body wall muscle (MYO4_CAEEL; P02566); aa_striated, *Aequipecten irradians* (scallop) striated muscle (MYS_AEQUIR, P24733). This figure was prepared with ESPript (33).

stabilization often stems from salt bridges between surface residues of neighboring chains, e.g., the g and e′ positions of consecutive heptads. Coiled-coil formation is a cooperative phenomenon, requiring a critical fragment length for stability.

The S2 subfragment of myosin II is an example of a sequence that has evolved to display a fine balance between coiled-coil propensity and structural instability. Different muscle types have fine-tuned S2 stability to different extents, as evidenced by the observation that N-terminal fragments of native scallop myosin S2 shorter than 340 residues fail to dimerize (13), whereas the 126-residue fragment of human cardiac β-myosin II described here, S2-Δ, can be isolated as a stable dimer after expression in *Escherichia coli* (5). A comparison of S2 sequences from different species and tissues reveals strong sequence variation in the first three heptads; however, overall features such as charge distribution or the positioning of noncanonical residues in a and d positions are relatively conserved (Fig. 1). This similarity presents an opportunity to decipher general principles of S2 design from the structure of a more stable representative like S2-Δ, the object of this study.

S2-Δ is remarkable in that both WT- and E924K-S2-Δ form nearly straight canonical coiled coils (Fig. 2), even though only a few stabilizing interchain salt bridges are present, and its a/d positions are occupied by atypical residues in a significant number of cases, especially toward the N terminus. With 190-Å length and only 25-Å width, this is one of the most elongated structures reported at this resolution hitherto. WT- and E924K-S2-Δ have very similar overall structures, and differences are caused by different crystal packing environments rather than by the single point mutation. In WT-S2-Δ, a polar crystal contact between E916 from a neighboring molecule and the backbone amide of M852 disrupts the N terminus, leading to disorder of the first 12 residues in one chain and straightening of the other due to the absence of coiled-coil interactions. Residual density indicates that the disordered chain protrudes from the main coiled-coil axis at an angle of ≈90° (Fig. 2). This flexibility point corresponds well to the structure of scallop S2N51, in which a similar part of the N terminus was too flexible to be observed (9). The situation is different in the E924K-S2-Δ mutant. These crystals contain two molecules per asymmetric unit; the crystal packing places neighboring molecules head to tail, and the N and C termini stabilize each other (see Fig. 5, which is published as supporting information on the PNAS web site), leading to preservation of coiled-coil geometry over the complete sequence. Both termini are splayed, and it is not clear whether this is a consequence of crystal packing or folding properties of the S2-Δ fragment. However, whereas the increase in coiled-coil radius at the C terminus may reflect the fading that is also seen at the termini of other coiled-coil structures, the extensive intramolecular hydrogen bonding pattern found at the N terminus argues strongly for a specific feature of S2 (Fig. 3). The observation of different structures of the N terminus of S2, ranging from disordered in scallop S2N51 (9) to partially ordered/α-helical (WT-S2-Δ) to coiled coil (E924K-S2-Δ), indi-

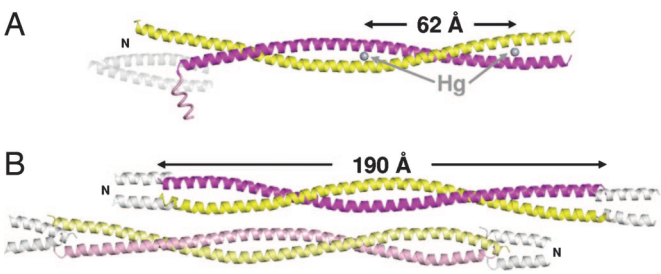

Fig. 2. Ribbon plots of the asymmetric unit of (*A*) WT-S2-Δ and (*B*) E924K-S2-Δ. N designates the N terminus. Light-gray ribbons depict crystallographic neighbors. In *A*, dark-gray spheres show the position of two mercury atoms bound to C905 and C947. The pink helical coil indicates the position of residual electron density at the flexible N terminus of the chain in magenta. All molecular representations were prepared with PyMOL (34).

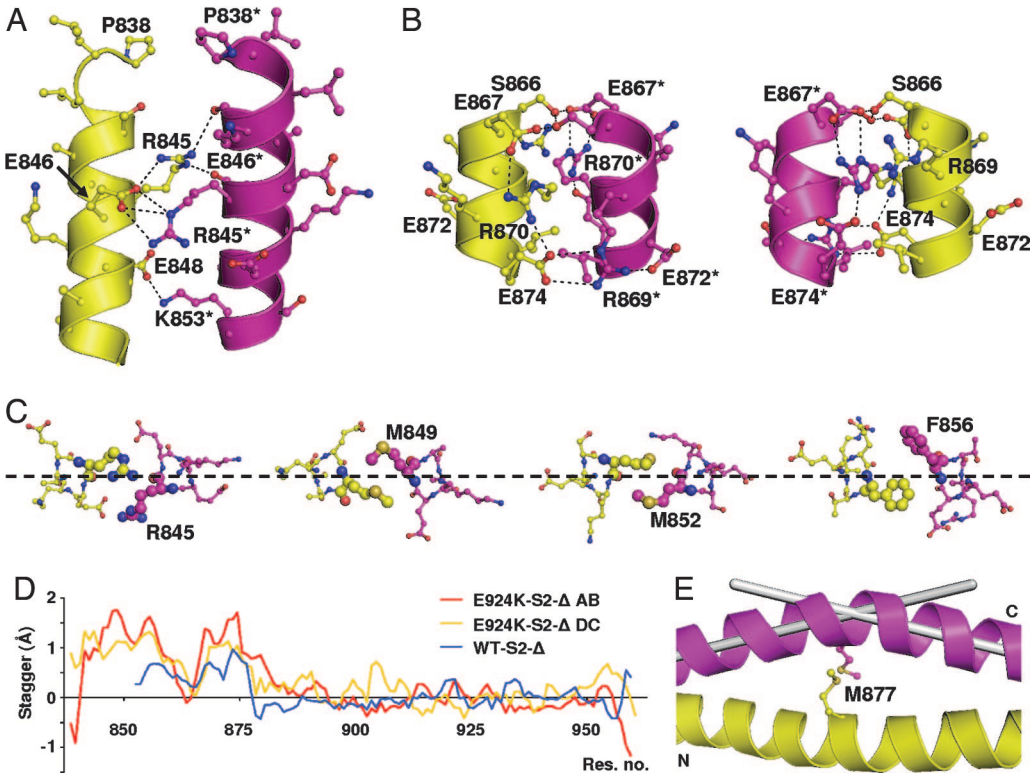

Fig. 3. Local asymmetry in S2-Δ. (*A*) Hydrogen-bonding network at the N terminus of E924K-S2-Δ. (*B*) Asymmetric hydrogen bonding network around R869 shown from ''front'' and ''back'' of WT-S2-Δ. (*C*) Asymmetry of N-terminal noncanonical a/d residues of E924K-S2-Δ. The dashed lined connects the center of the two α-helices and thus defines the expected twofold dimer axis. (*D*) Local stagger along WT- and E924K-S2-Δ, calculated from trace positions determined with TWISTER (35). (*E*) Kink at M877 in WT-S2-Δ.

cates that only a small energy barrier needs to be overcome to induce different structural states in the first dozen residues. This small barrier may help in reconciling previous studies that demonstrated the necessity for the presence of the labile native S2 sequence in generating a full powerstroke (14) but found uncoiling limited to only a small part of S2 in two-headed rigor binding to actin (3, 15).

The structure of S2-Δ reveals a number of interhelical salt bridges. These, however, are not observed in all of the positions predicted from sequence analysis, and they are also not implemented symmetrically in the majority of cases. For example, in WT-S2-Δ R869 of chain B interacts with E874 of chain A, but the conformation of R869 in chain A and of E874 in chain B is different, preventing g–e′ salt bridge formation (Fig. 3). R869 of chain A interacts with polar residues from a crystallographic neighbor instead, and the asymmetrical salt bridge pattern at this position could therefore be a crystallization artifact. The anisotropic environment provided by packing into the thick filament could have a similar effect on solvent-exposed residues. In addition, R869 and R870 lie in the N-terminal asymmetry zone that extends approximately to M877 and is discussed below.

It is possible that S2-Δ is further stabilized through disulfide bridges of the two cysteine residues at the a positions 905 and 947. The residues are positioned appropriately, and in fact the electron density indicates that a disulfide bridge exists at C947 in E924K-ΔS2. In contrast, the cysteines at position 905 are not connected, but this could be an effect of radiation damage (16, 17).

Structural Asymmetry. Local asymmetry is not restricted to surface residues but is also observed in the hydrophobic core of S2-Δ. Inspection of the larger noncanonical residues in a and d positions shows that most of them are arranged asymmetrically around the coiled-coil main axis due to space constraints. This is particularly apparent at the N terminus of S2-Δ, where R845, M849, M852, and F856 are all nonequivalent with respect to their partners in the second monomer (Fig. 3). As these four residues interact with each other, a defined asymmetric core structure is generated, as evidenced by similar asymmetry patterns of the two crystallographically independent copies of E924K-S2-Δ. The occurrence of noncanonical amino acids at equivalent positions of the N termini of other S2 sequences is relatively conserved (Fig. 1).

The departure from strict two-fold rotational symmetry may be important, because it could contribute to the defined nonequivalence of the two S1 heads in the filament mentioned above. Disruption of twofold symmetry in dimeric coiled coils as a consequence of placing clusters of atypical residues at a and d positions has also been discussed extensively for the structure of tropomyosin (18). In tropomyosin, however, leucine residues are replaced by alanine, which is small and coiled-coil destabilizing rather than large and stabilizing like the residues found in S2-Δ (19, 20). In tropomyosin, the alanine clusters lead to local axial shift of the two α-helices (''stagger'') and to local bending of the coiled-coil axis. Similar effects are observed in S2-Δ. Significant staggering is found from the N terminus to residue M877 (Fig. 3), although here it is not a consequence of unoccupied space in the coiled core but of increased space requirement of the bulky residues, pushing each other out of the way. The stagger reaches a maximum value of 1.8 Å at M849 of E924K-S2-Δ and is less developed in the WT structure. Interestingly, WT-S2-Δ displays a distinctive kink at residue M877, which marks the end of the N-terminal asymmetry zone (Fig. 3). It is tempting to speculate that the varying degree of N-terminal disorder and the different extent of local asymmetry observed in the structures of WT- and

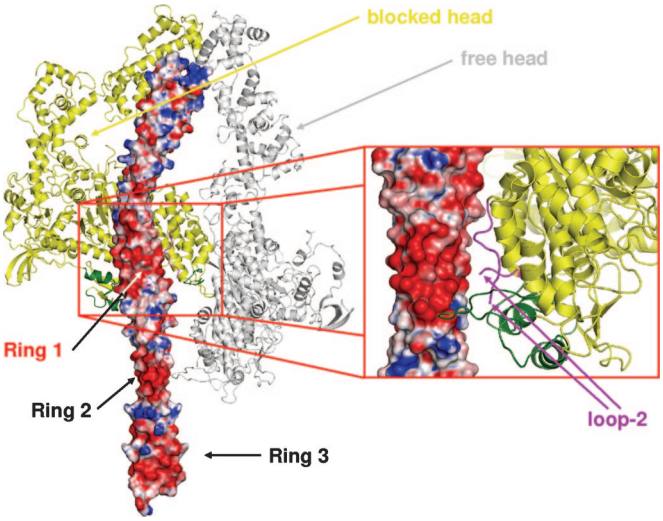

Fig. 4. Model of the OFF state, based on the structure of S2-Δ, a model of smooth muscle myosin in the 10S conformation (29) and the cryo-EM reconstruction of tarantula thick filament (2). The model was constructed by introducing a single bent at position 877 into S2-Δ. The electrostatic surface potential of S2-Δ was calculated with APBS (36). The blocked head is shown in yellow with the amino acids framing loop 2 shown in magenta, although the actual residues of loop 2 are missing. The remaining residues of the approximate actin-binding interface have been colored in dark green (37). (*Inset*) Magnification of the interaction after a clockwise 90° rotation around the coiled-coil main axis. For an unobstructed view, the free head has been omitted.

E924K-S2-Δ are functionally correlated. To corroborate this hypothesis, high-resolution structures of myosin constructs containing both S1 heads attached to fragments of S2 and trapped in different states of the crossbridge cycle will be required.

Electrostatic Properties. Another striking feature of S2-Δ is the charge distribution along its coiled-coil axis. Clusters of acidic residues generate three distinctive negative charge belts (approximately positions E894–D906, E921–E935 and E944–E958) interrupted by zones of neutral or moderately positive character (Fig. 4). This is a consequence of an underlying 28-residue repeat that dominates the LMM part of myosin II (21, 22). The charge distribution within these repeats is important for thick filament assembly, as is evidenced by the pH and salt dependence of myosin association in solution (23, 24) and by the axial 143-Å helical rise observed in the relaxed thick filament (25). This rise corresponds to an interaction of neighboring LMM tails after 3.5 28-residue repeats, arranging positive and negative patches next to each other.

The acidic clusters within S2 are highly conserved (Fig. 1) and probably play a functional role. In certain muscle types, relaxed myosin adopts a characteristic conformation, termed the OFF state, in which one crossbridge, the blocked head, folds back toward S2, and the second crossbridge rests on top of the first. This OFF state has been observed in vertebrate smooth (26), scallop striated (27), and tarantula striated muscle (2). In the OFF state, a regulatory loop within the actin-binding interface ("loop-2"; residues 625–647 in chicken skeletal muscle) of the blocked head would lie close to S2 (2, 28), but because of the lack of a suitable S2 structure, this interaction has not been further characterized hitherto. We have therefore constructed a model (Fig. 4) by fitting our S2-Δ structure and a model of the 10S conformation of smooth muscle myosin (29) into the 3D cryo-EM reconstruction of the tarantula thick filament (2). Although this does not allow us to analyze the contact in atomic detail, it identifies S2's first ring of negative potential centered around E900 as the interaction partner of loop 2 in S1. Intriguingly, this loop possesses a patch of conserved positively charged residues (28), suggesting that electrostatic interactions play an important role in stabilizing the OFF state. The first negative charge belt of the S2 subfragment contains a conserved D/E-X-EE sequence motif (Fig. 1), which may represent a regulatory sequence. Our model may therefore explain why not only a critical length of 15 coiled-coil heptad repeats but also the native sequence was required to obtain a fully regulated construct of smooth muscle myosin (4). The existence of a specific regulatory sequence motif or register within smooth muscle S2, however, has been questioned (30, 31).

The OFF state has until now only been observed in myosin-regulated muscles, which become activated on phosphorylation or Ca^{2+}-binding to myosin. In contrast, cardiac and skeletal muscles are actin-regulated, their activation depending on binding of Ca^{2+} to troponin. There is evidence for an intrinsic asymmetry in the myosin of these muscles as well, however (32). In addition, because the negatively charged residues of S2 and the patch of basic amino acids within the actin-binding loop are conserved, a similar electrostatic interaction may occur.

FHC-Associated Mutations Within S2-Δ. Several mutations within S2-Δ lead to hereditary heart disorders collectively termed FHC (8). Whereas some of these mutations, such as R869C or R870H, apparently affect structural integrity by disrupting side-chain hydrogen-bonding networks, several others lead to charge inversion and cluster within the second negative charge belt centered around residue E927 (Fig. 1). Comparison of the structures of WT- and E924K-S2-Δ demonstrates that these mutations are unlikely to have a structural effect. Instead, FHC mutation E924K was shown to lead to a loss of binding to the regulatory C1C2 fragment of MyBP-C (5), implicating the second negative charge belt in ΔS2 as the interaction partner of C1C2. It is conceivable that the charge-inverting mutations E927K, E930K, and E935K have a similar effect. The cardiac isoform of MyBP-C is involved in the control of sarcomere contractility depending in part on phosphorylation of C1C2 (7). The available data thus indicate that electrostatic interactions play a role in the regulatory function of cardiac MyBP-C.

Taken together, the structures presented here provide insight into how S2 balances stability and flexibility, and how these features are linked to mechanisms of asymmetry generation in myosin II. The obvious nonuniformity of charge distribution on the surface of S2 suggests that electrostatic interactions are important not only for assembly of the thick filament but also in the regulation of muscle activity.

Materials and Methods

WT- and E924K-S2-Δ were expressed in *E. coli* and purified in two steps, as described (5). The fragment starts with an invariant proline (P838) marking the C terminus of the regulatory domain of S1 and extends over the first 18 coiled-coil heptad repeats, ending at K963. Crystallization was achieved at 276 K with the vapor diffusion sitting-drop method. The optimized precipitant contained 16% (wt/vol) PEG 3350/200 mM trilithium citrate/100 mM Tris·HCl, pH 8.5, for WT-S2-Δ and 16% (wt/vol) PEG 3350/160 mM sodium acetate/200 mM Tris·HCl, pH 7.5, for E924K-S2-Δ. Best results were obtained with Emerald Clover sitting-drop plates. Crystals of WT-ΔS2 belong to space group $C222_1$ with unit cell dimensions of 40, 46, and 374 Å; E924K-S2-Δ crystallized in space group P1 with a = 34, b = 42, and c = 112 Å; $\alpha = 90.1$; $\beta = 95.4$ and $\gamma = 109.6°$, which changed to a = 41, b = 42 and c = 96 Å; $\alpha = 94.5$; $\beta = 92.0$ and $\gamma = 106.0°$ on soaking with heavy atom salts (see also Fig. 6, which is published as supporting information on the PNAS web site). Cryoprotection was achieved by briefly washing crystals in mother liquor supplemented with 5% (wt/vol) and then 15% (wt/vol) PEG-MME 5000. Final data sets were collected at 100 K at the

European Synchrotron Radiation Facility, Grenoble, France (see Table 1, which is published as supporting information on the PNAS web site, for details).

The WT structure was phased with two-wavelength MAD data collected at the absorption peak (LI) and inflection point (LIII) of a mercury derivative. E924K-S2-Δ (unit cell after heavy atom soaking) was solved by an unusual approach using anomalous data from a mercury derivative to locate heavy atom positions and a brute-force search with the WT structure to derive the relative orientation of two coiled coils contained in the asymmetric unit (see Figs. 7 and 8, which are published as supporting information on the PNAS web site). WT-S2-Δ was refined to an R factor of 24.2% (R_{free} 28.3%) at 2.7 Å; E924K-S2-Δ (crystal form after soaking) was refined to an R factor of 27.3% (R_{free} 34.9%) at 2.5 Å (see Table 1 and *Supporting Text*, which are published as supporting information on the PNAS web site, details). The native E924K-S2-Δ crystal form (unaltered cell parameters before soaking) was solved by molecular replacement, but the model was not fully refined, because packing and overall structure are highly similar to E924K-S2-Δ after soaking, and the diffraction data were of lower quality (data not shown). Data collection and refinement statistics are collected in Table 1. For full experimental details, refer to *Supporting Text*.

We are grateful to Axel Scheidig, Mathias Gruen, and Kristina Djinovic-Carugo for help during the initial stages of the project, and to Nathalie Bleimling for excellent technical assistance in protein purification. We thank Kenneth A. Taylor (Florida State University, Tallahassee, FL) for providing coordinates of a refined model of 10S smooth muscle myosin and Roger Craig (University of Massachusetts, Worcester, MA) for giving us access to the 3D reconstruction of tarantula thick filament. We further acknowledge the beamline staff at the European Synchrotron Radiation Facility (Grenoble, France), the Deutsches Elektronensynchrotron (Hamburg, Germany), and Elettra (Trieste, Italy) for help during data collection and Roger S. Goody for generous support. This project was financed by grants from the Deutsche Forschungsgemeinschaft (to M.G. and I.S.).

1. Geeves MA, Holmes KC (2005) *Adv Protein Chem* 71:161–193.
2. Woodhead JL, Zhao FQ, Craig R, Egelman EH, Alamo L, Padron R (2005) *Nature* 436:1195–1199.
3. Chakrabarty T, Xiao M, Cooke R, Selvin PR (2002) *Proc Natl Acad Sci USA* 99:6011–6016.
4. Trybus KM, Freyzon Y, Faust LZ, Sweeney HL (1997) *Proc Natl Acad Sci USA* 94:48–52.
5. Gruen M, Gautel M (1999) *J Mol Biol* 286:933–949.
6. Gruen M, Prinz H, Gautel M (1999) *FEBS Lett* 453:254–259.
7. Kunst G, Kress KR, Gruen M, Uttenweiler D, Gautel M, Fink RH (2000) *Circ Res* 86:51–58.
8. Fung DC, Yu B, Littlejohn T, Trent RJ (1999) *Hum Mutat* 14:326–332.
9. Li Y, Brown JH, Reshetnikova L, Blazsek A, Farkas L, Nyitray L, Cohen C (2003) *Nature* 424:341–345.
10. Kammerer RA, Schulthess T, Landwehr R, Lustig A, Engel J, Aebi U, Steinmetz MO (1998) *Proc Natl Acad Sci USA* 95:13419–13424.
11. Harbury PB, Kim PS, Alber T (1994) *Nature* 371:80–83.
12. Lupas AN, Gruber M (2005) *Adv Protein Chem* 70:37–78.
13. Málnási-Czismadia A, Shimony E, Hegyi G, Szent-Györgi AG, Nyitray L (1998) *Biochem Biophys Res Commun* 252:595–601.
14. Lauzon AM, Fagnant PM, Warshaw DM, Trybus KM (2001) *Biophys J* 80:1900–1904.
15. Chakrabarty T, Yengo C, Baldacchino C, Chen LQ, Sweeney HL, Selvin PR (2003) *Biochemistry* 42:12886–12892.
16. Weik M, Ravelli RB, Kryger G, McSweeney S, Raves ML, Harel M, Gros P, Silman I, Kroon J, Sussman JL (2000) *Proc Natl Acad Sci USA* 97:623–628.
17. Burmeister WP (2000) *Acta Crystallogr D* 56:328–341.
18. Brown JH, Cohen C (2005) *Adv Protein Chem* 71:121–159.
19. Kwok SC, Hodges RS (2004) *J Biol Chem* 279:21576–21588.
20. Tripet B, Wagschal K, Lavigne P, Mant CT, Hodges RS (2000) *J Mol Biol* 300:377–402.
21. Parry DA (1981) *J Mol Biol* 153:459–464.
22. McLachlan AD, Karn J (1982) *Nature* 299:226–231.
23. Davis JS (1988) *Annu Rev Biophys Chem* 17:217–239.
24. Tsunashima Y, Akutagawa T (2004) *Biopolymers* 75:264–277.
25. Squire JM, Al Khayat HA, Knupp C, Luther PK (2005) *Adv Protein Chem* 71:17–87.
26. Wendt T, Taylor D, Trybus KM, Taylor K (2001) *Proc Natl Acad Sci USA* 98:4361–4366.
27. Stafford WF, Jacobsen MP, Woodhead J, Craig R, O'Neall-Hennessey E, Szent-Györgi AG (2001) *J Mol Biol* 307:137–147.
28. Rovner AS (1998) *J Biol Chem* 273:27939–27944.
29. Liu J, Wendt T, Taylor D, Taylor K (2003) *J Mol Biol* 329:963–972.
30. Ikebe M, Yamada M, Mabuchi K, Kambara T, Ikebe R (1998) *Biochemistry* 37:13285–13290.
31. Ikebe M, Yamada M, Mabuchi K, Kambara T, Ikebe R (1999) *Biochemistry* 38:10768–10774.
32. Harris SP, Heller WT, Greaser ML, Moss RL, Trewhella J (2003) *J Biol Chem* 278:6034–6040.
33. Gouet P, Robert X, Courcelle E (2003) *Nucleic Acids Res* 31:3320–3323.
34. DeLano WL (2002) in *The PyMOL User's Manual* (DeLano Scientific, San Carlos, CA).
35. Strelkov SV, Burkhard P (2002) *J Struct Biol* 137:54–64.
36. Baker NA, Sept D, Joseph S, Holst MJ, McCammon JA (2001) *Proc Natl Acad Sci USA* 98:10037–10041.
37. Geeves MA, Fedorov R, Manstein DJ (2005) *Cell Mol Life Sci* 62:1462–1477.